Atmos. Meas. Tech., 7, 409–418, 2014
www.atmos-meas-tech.net/7/409/2014/
doi:10.5194/amt-7-409-2014

Atmospheric Measurement Techniques
Open Access

Properties of rainfall in a tropical volcanic island deduced from UHF wind profiler measurements

A. Réchou[1], T. Narayana Rao[2], O. Bousquet[1], M. Plu[1,3], and R. Decoupes[4]

[1]Laboratoire de l'Atmosphère et des Cyclones, UMR8105 CNRS, Météo France, Université de la Réunion, Réunion Island, France
[2]National Atmospheric Research Laboratory, Gadanki, India
[3]CNRM-GAME, UMR3589, CNRS and Météo-France, Toulouse, France
[4]Université de la Réunion, UMS3365, OSUR, Saint Denis, Réunion Island, France

Correspondence to: A. Réchou (arechou@univ-reunion.fr)

Received: 14 March 2013 – Published in Atmos. Meas. Tech. Discuss.: 4 April 2013
Revised: 25 November 2013 – Accepted: 2 January 2014 – Published: 7 February 2014

Abstract. The microphysical properties of rainfall at the island of Réunion are analysed and quantified according to one year of wind profiler observations collected at Saint-Denis international airport. The statistical analysis clearly shows important differences in rain vertical profiles as a function of the seasons. During the dry season, the vertical structure of precipitation is driven by trade wind and boundary-layer inversions, both of which limit the vertical extension of the clouds. The rain rate is lower than 2.5 mm h^{-1} throughout the lower part of the troposphere (about 2 km) and decreases in the higher altitudes. During the moist season, the average rain rate is around 5 mm h^{-1} and nearly uniform from the ground up to 4 km.

The dynamical and microphysical properties (including drop size distributions) of four distinct rainfall events are also investigated through the analysis of four case studies representative of the variety of rain events occurring on Réunion: summer deep convection, northerly-to-northeasterly flow atmospheric pattern, cold front and winter depression embedded in trade winds. Radar-derived rain parameters are in good agreement with those obtained from collocated rain gauge observations in all cases, which demonstrates that accurate qualitative and quantitative analysis can be inferred from wind profiler data. Fluxes of kinetic energy are also estimated from wind profiler observations in order to evaluate the impact of rainfall on soil erosion. Results show that horizontal kinetic energy fluxes are systematically one order of magnitude higher than vertical kinetic energy fluxes. A simple relationship between the reflectivity factor and vertical kinetic energy fluxes is proposed based on the results of the four case studies.

1 Introduction

Soil erosion is a complex problem that can significantly impact the activities of humans and wildlife, vegetation, and infrastructures. It involves many spatially and temporally varying aspects of rainfall such as drop size distribution (DSD) and intensity, wind speed, surface water (both standing and flowing), as well as vegetation cover and soil characteristics (Brian, 2000; Kinnell, 2005; Iserloh et al., 2013). Properties that determine the soil erodibility factor such as soil aggregation, shear strength, rain intensity, and DSD are subject to important seasonal variability (Romkens et al., 1990; Rosenfeld and Ulbrich, 2003; Rao et al., 2009). Changes occurring between and during rainstorms can also significantly affect the incidence and intensity of rill and interrill erosion and, therefore, both short- and long-term hill-slope erosional response. In this respect, a precise characterization of rainfall properties and variability is required in order to better represent the impact of precipitation on erosion. This is particularly true in the tropics, where heavy rainfall tends to significantly transform the landscape.

During the Taiwan Area Mesoscale Experiment (TAMEX), Johnson and Bresch (1991) examined the

characteristics of rainfall distributions in Taiwan using soundings, surface precipitation data and radar observations. One outcome of this experiment was to show that heavy rainfall events were generally associated with either deep convective (prefrontal or frontal) or stratiform (essentially postfrontal) precipitation systems connected to mid-latitude disturbances. The seasonal changes of the prevailing wind (namely trade winds) and atmospheric stability were also found to play an important role in the properties and distribution of rainfall. The impact of trade winds on precipitation is not surprising, as this phenomenon is a fundamental component of atmospheric circulation in this part of the world. Similar results were later found in Hawaii, where trade winds prevail 85–95 % of the time during the summer and 50–80 % of the time during winter (Sanderson, 1993), and more recently in the Caribbean, during the Dominica experiment (Smith et al., 2012). A few studies aimed at describing the spatial variability of rainfall have also been conducted in the Southern Hemisphere, in particular on Réunion, a small, heavily populated, volcanic island located in the South-Western Indian Ocean (SWIO) (Barcelo et al., 1997; Baldy et al., 1996; Taupin et al., 1999). The vertical structure of trade winds over Réunion was also investigated by Lesouëf (2010) and Lesouëf et al. (2011), although these authors did not investigate potential relationships between atmospheric circulation and rainfall properties.

The island of Réunion is one of the rainiest areas on earth and holds all rainfall world records for periods ranging from 12 h to 15 days. It is regularly affected by torrential flash floods, landslides and solid transport in river flow, and is thus particularly subject to erosion processes due to its fragile volcanic soil. In this regard, this island represents an ideal natural laboratory to learn more about the properties of precipitation in the tropics, as well as to evaluate the impact of rainfall on soil erosion. The recent deployment of a wind profiler on the island enables, for the first time, a thorough investigation of the space and time structure of rainfall in the SWIO area; the wind profiler also represents an important asset to examine the microphysical properties of rainfall in the tropics.

The ability of wind profilers (UHF or VHF) to estimate rainfall properties was demonstrated by several investigators (e.g., Wakasugi et al., 1986; Rajopadhyaya al., 1993) using a variety of techniques. Gossard (1988) and Gossard et al. (1990) used a UHF profiler to retrieve DSD in light rain. Williams (2002) used the SANS Air Motion (SAM) model to derive vertical profiles of air motion, spectral width and DSD from UHF Doppler spectra and obtained reliable results for drop diameter greater than 1.5 mm. Cifelli et al. (2000) and Schafer et al. (2002) used a dual-frequency method based on collocated UHF and VHF measurements, to estimate rain rate (R) and DSD. Subsequently, Kanofsky and Chilson (2008) quantified the error in DSD retrievals and rain bulk parameters in central Oklahoma using UHF wind profiler measurements and 2-D video disdrometer data.

The aim of the present study is to evaluate the microphysical properties of rainfall in Réunion using one year of collocated wind profiler and rain gauge observations. The overarching objective is to facilitate the quantification of kinetic energy flux by raindrop and wind, which is the key to quantifying the effect of precipitation on soil erosion. Indeed, erosion models often ignore the fact that the eroding surface has a microtopography, which forces water to flow though a series of shallow pools where material is transported by raindrop-induced flow (Kinnell, 2005). The kinetic energy estimates used to represent this transport in model simulations are often small compared to experimental values that can be found in the literature (Iserloh et al., 2013).

The article is organized as follows: an overview of the geographical and climatological characteristics of Réunion is given in Sect. 2. Section 3 describes the data and methodology used to estimate DSD and kinetic energy fluxes. The mean precipitation characteristics during wet and dry seasons are presented in Sect. 4 together with a detailed analysis of four typical cases representative of the main weather patterns occurring at Réunion. Vertical and horizontal kinetic energy fluxes are estimated from DSD and wind data and a relationship between the reflectivity factor Z and vertical kinetic energy flux is proposed for each case study.

2 The island of Réunion

The island of Réunion (Fig. 1) emerges from sea level as two volcanic summits originating from the same hot spot, which explains its roughly circular shape of 60 km mean diameter with a peak altitude of 3000 m. Intense erosion due to the fragile volcanic soil and heavy precipitation have led to a steep orography. The lava plateau, linearly inclined towards the sea, overhangs sub-vertical ramparts of kilometric size, which borders ancient craters (a.k.a. cirques). Due to its geographical location (21° S, 55° E), Réunion is influenced by tropical and subtropical climates. During summer, which extends from December to February, the Intertropical Convergence Zone (ITCZ) is close to the island, resulting in high relative humidity and weak trade winds that favour the formation of deep convective systems. During winter (June to August), the subtropical upper level jet stream is closer to Réunion (Hastenrath, 1991), leading to strong trade winds and weak relative humidity conditions. Trade winds prevail throughout the year, but significantly intensify from April to September (Baldy et al., 1996). As part of the Hadley cell circulation, easterly winds prevail in the lower levels while westerly winds prevail in upper levels. Lesouëf (2010) and Lesouëf et al. (2011) have shown that the trade wind inversion generally occurs around 2.5 km above mean sea level (a.m.s.l.) during the austral summer and between 2.4 and 3 km a.m.s.l. during the rest of the year.

Fig. 1. Topography of Réunion. The UHF wind profiler is located at Saint-Denis Airport (20°53′33″ S, 55°31′44″ E). Red circles indicate the locations of principal cities.

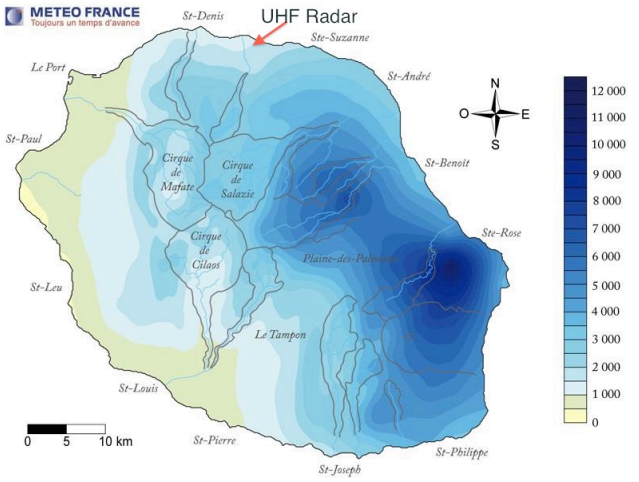

Fig. 2. Mean annual rainfall (mm) on Réunion over a 20 yr period starting in 1981. Precipitation estimates are derived from rain gauge data taken throughout the island.

Cloud formation follows a strong diurnal cycle. Orographic forcing is responsible for stronger precipitation on the eastern, leeward, coast (Fig. 2). Precipitation is generally higher over the high reliefs than close to the coast (Fig. 2). The maximum of precipitation occurs between 1000 m and 2000 m a.m.s.l. Precipitation regimes in Réunion can be divided into two main seasons. The warm, moist, season extends from November to April and is associated with deep convection, sometimes in relation with tropical cyclones. The most intense precipitation events occur during this period, sometimes reaching world records (Quetelard et al., 2009). The cool, dry, season extends from May to October, and corresponds to the period when the island is mainly influenced by southeasterly trade winds. At this time of the year, the polar-front jet can penetrate to subtropical latitudes, and merge with the subtropical jet to form a single band (Postel and Hitchman, 2001). These phenomena may occasionally reach Réunion and generate intense frontal precipitation events.

3 Data and methodology

3.1 Radar data

The UHF radar and the rain gauge used in this study are both deployed at Saint-Denis international airport, on the northern coast of the island. This location corresponds to an intermediate area between the dry western zone and the eastern rainy zone (Fig. 2). The UHF wind profiler (Degreane Horizon PCL1300) provides vertical profiles of reflectivity, wind, spectral width and skewness every five minutes. In order to retrieve the three components of the wind, the profiler alternatively uses one vertical and four oblique beams, with a one-way half-power aperture of 8.5°. The oblique beams, with an off-zenith angle of 13°, are disposed every 90° in azimuth. The zenith-pointing beam radial velocity provides the air vertical velocity during fair weather and Doppler velocity of hydrometeors in precipitation. The horizontal wind components are inferred from both oblique and vertical beam measurements under the assumption of horizontal wind local homogeneity. During an acquisition cycle, data collection is achieved in two modes – the low-altitude (high resolution) and high-altitude (low resolution) modes. The difference between low altitude and high altitude modes is related to the pulse width (300 m vs. 750 m) and repetition frequency (22.22 KHz vs. 12.34 KHz). The low mode has a 75 m vertical resolution and provides observations up to 6750 m (note that this height is indicative and can vary depending upon humidity and turbulence conditions), whereas the high mode has a 150 m vertical resolution and allows measurements up to 12 000 m.

Profilers receive backscatter returns from both atmospheric (e.g., precipitation) and non-atmospheric (e.g. birds) sources. The first step in wind profiler data analysis is thus to discriminate between those two sources so as to be able to discard all non-atmospheric returns. In order to do this, a large number of consecutive samples are integrated (in the Fourier space) to increase the signal-to-noise ratio of atmospheric signal. This task is performed for each range gate and for each of the five transmitted beam directions. After this first step, called coherent integration, the four strongest peaks in the resulting spectrum are examined to determine the peaks that are likely to be associated with atmospheric returns. This is done through the application of an ensemble of selection criteria based upon the value and space-time continuity of radial velocity, power and spectral width measurements. Particular care is devoted to the detection and correction of bimodal peaks resulting, for instance, from the concatenation of atmospheric and ground clutter echoes, contamination from birds, radio frequency interference or other sources.

3.2 DSD retrieval

The measurement of precipitation by UHF radar is achieved by mapping the Doppler velocity spectrum into diameter space by assuming that measured velocity is solely due to the hydrometeor fall speed. Vertical ambient air motion and atmospheric turbulence are thus considered to be negligible, and Rayleigh scatter from particles is considered the essential contribution to the signal. This assumption of negligible vertical air motion, which is valid in stratiform precipitation, fails, however, in convection. Kanofsky and Chilson (2008) found that the largest errors in rain-rate estimates are due to unaccounted vertical ambient air motion. This error can nevertheless be significantly reduced by performing a spectral average over 3 radar cycles (~ 15 min).

The DSD is estimated from the Doppler spectrum at each range gate by applying a specific relationship between the drop diameter and the terminal fall speed. From the retrieved DSD, it is then possible to determine the vertical profile of the radar reflectivity factor, the median volume drop diameter rainfall rate, and kinetic energy fluxes. The above parameters are estimated from the set of Eqs. (1)–(9) given hereafter.

First, we assume that, on average, the raindrop size distribution $N(D)$, where D is the diameter, follows a gamma function (Eq. 1, Ulbrich, 1983). The gamma function is known to accurately describe a larger variety of DSD (Kozu and Nakamura, 1991; Su and Chu, 2007) and to improve the accuracy of R (Ulbrich and Atlas, 1998).

$$N(D) = N_o D^{\mu} e^{-\Lambda D}, \tag{1}$$

whereN_0 is the number density parameter ($\mathrm{m}^{-3}\,\mathrm{mm}^{-1-\mu}$), Λ is the slope parameter (mm^{-1}), and μ is a dimensionless shape parameter.

Equations (2) and (3) provide the raindrop fall speed in still air, taking into account the change of density with height (Atlas et al., 1973; Foote and du Toit, 1969).

$$W_f(D) = \alpha_1 - \alpha_2 e^{-\alpha_3 D} \tag{2}$$

$$\alpha_1 = 9.65(\rho_o/\rho)^{0.4} \quad \alpha_2 = 10.3(\rho_o/\rho)^{0.4} \quad \alpha_3 = 600 \tag{3}$$

From Eq. (4), which relates μ to Λ, one can reduce Eq. (1) to a two-parameter problem (Chu and Su, 2008).

$$\Lambda = 50.0\mu^2 + 1200.0\mu + 3390.0 \tag{4}$$

The mean vertical Doppler velocity and reflectivity factor, $< W_\mathrm{f} >$ (Eq. 5) and $< Z >$ (Eq. 6), are directly measured by the profiler at the resolution of the pulse volume. These parameters are deduced from Eqs. (1) and (2) after an integration over the diameter interval supposed to extend from 0 to infinity.

$$< W_\mathrm{f} > = \alpha_1 - \alpha_2(1 + \alpha_3/\Lambda)^{-(\mu+7)} \tag{5}$$

$$< Z > = N_o \Gamma(\mu+7)\Lambda^{-(\mu+7)} \tag{6}$$

The expression of the precipitation rate R (Eq. 7) is obtained from the same procedure.

$$R = N_o \Gamma(\mu+4)\pi 6^{-1}(\alpha_1 \Lambda^{-(\mu+4)} - \alpha_2(\Lambda+\alpha_3)^{-(\mu+4)}) \tag{7}$$

The rain kinetic energy flux crossing an horizontal surface of unit area during a unit of time is decomposed into a horizontal kinetic energy flux (HKEF), related to the raindrop entrainment by the wind velocity V (Eq. 8), and a vertical kinetic energy flux (VKEF), which is a function of the drop vertical velocity (Eq. 9). The value of Λ is obtained from Eqs. (4) and (5), which allows for the retrieval of N_o from Eq. (6).

$$\mathrm{HKEF} = \rho_\mathrm{w} V^2 R/2 \tag{8}$$

$$\begin{aligned}\mathrm{VKEF} = \rho_\mathrm{w} N_o \Gamma(\mu+4)\pi 12^{-1}[&\alpha_1^3 \Lambda^{-(\mu+4)} \\ &- \alpha_2^3(\Lambda+3\alpha_3)^{-(\mu+4)} \\ &+ 3\alpha_1\alpha_2^2(\Lambda+2\alpha_3)^{-(\mu+4)} \\ &- 3\alpha_2\alpha_1^2(\Lambda+\alpha_3)^{-(\mu+4)}],\end{aligned} \tag{9}$$

where ρ and ρ_w are air and water density, respectively, and Γ is the gamma function. MKSA units are used.

DSD retrieval is only performed for rain data. An approach similar to that proposed by Rao et al. (2008) is followed in order to identify rain echoes using specific criteria on Z and W_f. Echoes are classified as rain echoes when $Z > 10$ dBZ, $W_\mathrm{f} < -1\,\mathrm{m\,s}^{-1}$ and normalized skewness < -0.1. The reflectivity threshold is defined by comparing the occurrence of rain in rain gauge and in the lower levels of the UHF radar. The additional use of a threshold on skewness allows for the efficient removal of snow echoes.

3.3 Radar calibration

Radar calibration is an essential step in deriving DSD from a wind profiler. For power calibration, the radar backscatter at the error-free lowest range gate is usually compared to either disdrometer-derived Z/R or R obtained from a rain gauge. In the present study, the radar calibration is performed by comparing radar-derived rain rates with rain gauge data, separately for dry and wet seasons (Fig. 3). Steiner and Smith (2000) pointed out that uncertainties in radar and rain gauge measurements are related to the space–time resolution and coverage of observations, measurement errors, as well as to weather conditions (i.e. the variability of the raindrop size distribution). In this respect, it is important to determine the range of uncertainties associated with quantitative precipitation estimation.

The accuracy of rain gauge measurement depends both on the surface collection and on the nominal mass failover of the bucket. For an area of 1000 cm^2 and a mass of 20 g, this gives an amount of ~ 0.2 mm in height of water. The unit is set to minimize the error at low intensities of rainfall. For very

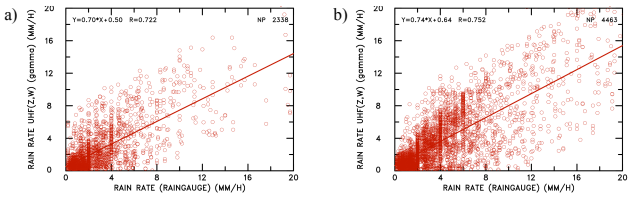

Fig. 3. Scatter plot of radar- and rain gauge-derived rain rate for the periods **(a)** May 2009–October 2009 (dry season) and **(b)** November 2009–April 2010 (moist season). Radar data are obtained between 400 and 500 m a.m.s.l. Rain gauge data are obtained at sea level.

high intensities ($> 150\,\mathrm{mm\,h^{-1}}$), the maximum error in R can reach $-10\,\%$ (the measure is always underestimated). It is corrected numerically by recent acquisition systems. Clark et al. (2005) observed that the primary source of uncertainty in calibrating a profiler from disdrometer or rain gauge measurements is related to the large reflectivity gradients in the first few hundred metres above the ground. To mitigate this error, radar data used in the calibration process are taken as close to the ground as possible, considering signal saturation, receiver linearity, and ground clutter contamination. In the present case, the best level was found to be between 400 m and 500 m.

It can be seen from Fig. 3 that R is larger during the moist season than during the dry season. Despite uncertainties in radar–rain gauge comparisons ensuing from the above described limitations, the correlation is > 0.7 for both seasons, which is a remarkable result. The spread of the scatter is mostly due to the existence of different wind regimes, as will be seen in the following section.

4 Results

4.1 Statistical analysis

Figure 4 presents the mean vertical profile of rain rate as derived from radar measurements between 0.4 and 3 km a.m.s.l. These statistics are built from samples of non-zero hourly rain rates and are compared to corresponding rain gauge data. During the dry season, the mean rain rate averages around $2.5\,\mathrm{mm\,h^{-1}}$ within the first two kilometres of the troposphere before decreasing at higher levels (Fig. 4a). The variability is relatively low (slightly higher above 2 km), although higher than the mean value throughout the observed vertical layer. An overall decrease of the rain rate with height can also be noticed. This observation is supported by surface rain gauge measurements which show higher rain rates at the ground than at the lowermost height given by the radar.

This result is quite unexpected, as one would expect a gradual decrease of rain rate with altitude due to strong low-level evaporation occurring during the dry season. The vertical profile of the corresponding wind patterns (Fig. 5)

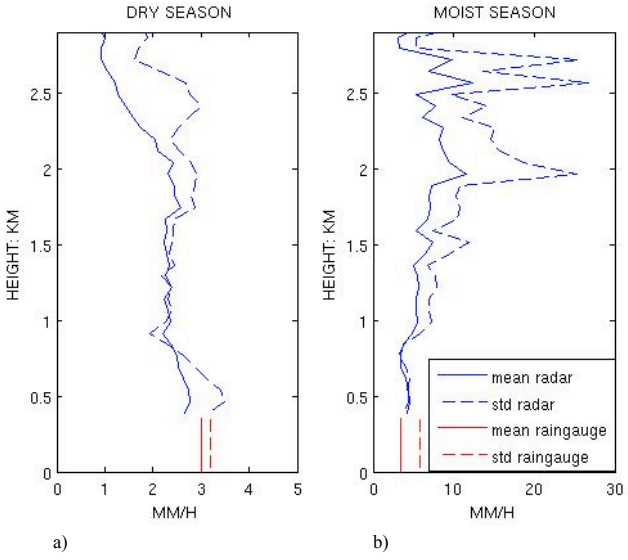

Fig. 4. Vertical profile of the mean (plain line) and standard deviation (dashed line) of the rain rate as derived from UHF radar measurements during **(a)** the dry season and **(b)** the warm season. Red lines show corresponding rain-gauge estimates at sea-level.

suggests that the trade wind inversion is probably responsible for the observed vertical structure of the rain rate. Indeed, the inversion of the trade winds around 3 km seems to prohibit the vertical development of convective clouds. Such a feature has already been observed in previous studies (e.g., Riehl, 1954; Augstein et al., 1973; Stevens, 2007).

During the moist season (Fig. 4b), the retrieved rain rate is higher at all heights and presents a regular increase with height, reaching $10\,\mathrm{mm\,h^{-1}}$ at 2 km a.m.s.l. Clear differences also exist in terms of event duration (not shown), with precipitation persisting longer (up to 6 to 8 h) during the moist season than during the dry season. The variability is also much higher than during the dry season, and can reach up to $25\,\mathrm{mm\,h^{-1}}$ at 2 and 3 km a.m.s.l. Also notice that the trade wind inversion is smoother and occurs at a higher level during the moist season (Fig. 5c–d), which is in good agreement with results of Lesouëf (2010). The overall variability observed in both seasons is related to the variety of precipitation systems affecting Réunion (see below). During the 2009–2010 moist season, Réunion was also affected by several tropical depressions, although none of them directly overpassed the studied area.

4.2 Case studies

In order to gain more information on precipitation systems that impinge on the island throughout the year, four distinct classes of weather patterns representative of the variety of rainfall events on Réunion are defined: frontal situations (FF), strong trade winds (ST), low pressure systems associated with tropical depressions (LP) and north to

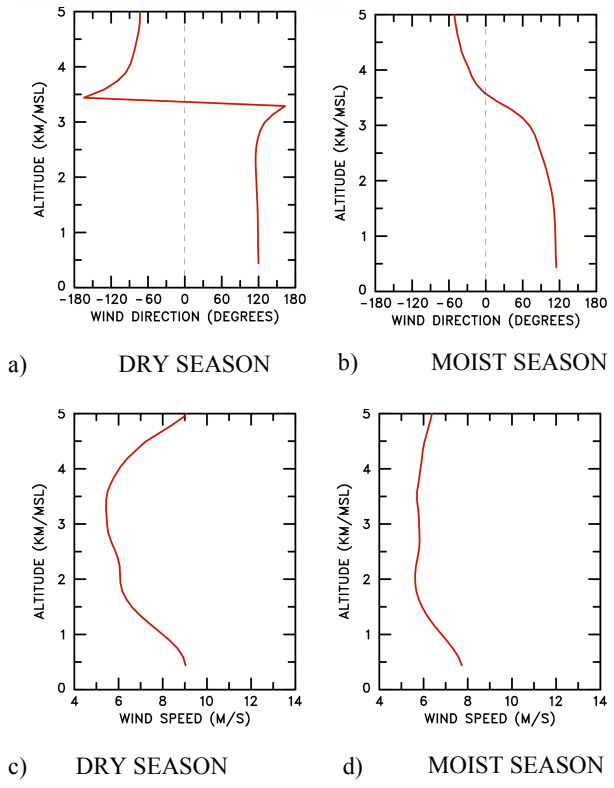

Fig. 5. As in Fig. 4, but for the mean wind direction **(a, b)** and intensity **(c, d)** during the dry season **(a, c)** and the moist season **(b, d)**.

north-easterly (NNE) flow situations. The two latter classes usually occur in summer and often lead to deep convection, while the two former patterns generally occur in winter. During the period of interest of this study, these weather patterns occurred cumulatively over 131 days. The FF and ST classes were slightly less frequent than the climatological average (24 and 46 days, respectively in comparison to climatological values of 30 and 53 days). During summer, the NNE pattern occurred on 40 days (highest number of cases during the last 32 yr), while the number of LP events was slightly smaller than the climatological value (21 days against the climatological value of 30 days). Among those 131 events, 89 were observed by the wind profiler.

In order to evaluate the efficiency of UHF radar rain retrieval under various meteorological situations, four specific days corresponding to each of the four weather patterns described above were selected: 27 June 2009, 19 August 2009, 2 February 2010 and 17 March 2010. The synoptic situation associated with these particular weather events can be inferred from the Meteosat images shown in Fig. 6. The 27 June 2009 event is associated with a cold frontal passage (FF) over the southern part of the island (Fig. 6a); the 19 August 2009 event corresponds to a case of strong trade wind inversion (ST) leading to the formation of low-level clouds over the island (Fig. 6b); on 2 February 2010 (LP case), Réunion is under the influence of the tropical cyclone Fami, located over Madagascar, whose rainbands extend eastwards toward the island (Fig. 6c); the fourth case study, on 17 March 2010, corresponds to a northerly to north-easterly flow situation (NNE) leading to the formation of deep convective clouds over Réunion (Fig. 6d).

Figure 7 presents height–time contours of reflectivity, vertical Doppler velocity, wind velocity and rain rate, deduced from UHF radar measurements collected during the two winter cases (i.e., on 27 June and 19 August 2009). On 27 June, precipitation was weak to moderate, although high values of reflectivity (reaching up to 40 dBZ) could sometimes be observed in relation to convective frontal precipitation (Fig. 7a). The corresponding vertical Doppler velocities (Fig. 7c) was always in the range of -6 to $-8\,\mathrm{m\,s^{-1}}$, which corresponds to small-to-medium size raindrops. A signature of the frontal pattern is visible in the horizontal wind contours (Fig. 7e), as a sloping structure. The retrieved rain rate (Fig. 7g) could reach up to $15\,\mathrm{mm\,h^{-1}}$ when convective precipitation passed over the radar, but it was generally weak.

On 19 August 2009, precipitation was mostly confined to lower altitudes (within 3 km above the ground) and was associated with low reflectivity values throughout the event (Fig. 7b). The observed vertical Doppler velocities were therefore relatively weak, and did not exceed $6\,\mathrm{m\,s^{-1}}$ (Fig. 7d). A well-defined trade wind inversion could be observed at ~ 4 km a.m.s.l. with easterly winds below and westerly winds above (Fig. 7f). These shallow clouds, which often prevail during winter, are mostly associated with strong trade winds. They formed in the eastern part of the island as a result of terrain induced forcing and are advected westward over the radar. Precipitation is restricted to below the trade wind inversion layer, which acts to prohibit the development of clouds. The present result is in good agreement with Smith et al. (2012), who noticed the existence of two main types of convection over Dominica. During periods of weak trade winds (in our case south to south-easterly wind direction, before 19:00 UTC in Fig. 7), diurnal thermal convection prevail causing leading to low precipitation ($R < 4\,\mathrm{mm\,h^{-1}}$). During periods of strong trade winds (SE'ly wind after 19:00 UTC in Fig. 7), mechanically forced convection over the windward slopes brought heavy rain to the high terrain ($> 7\,\mathrm{mm\,h^{-1}}$ up to 2 km).

In good agreement with results shown in Fig. 4, the two summer cases appear to be associated with more intense precipitation. On 2 February 2010 (LP weather pattern), the remnants of tropical cyclone Fami, which made landfall over Madagascar a day before, generated intense convection over Réunion island. High values of reflectivity (Fig. 8a) and vertical Doppler velocity (Fig. 8c) could be observed at all heights for more than one hour (14:00–15:15 UTC). The wind shear was also strong, especially before 16:30 UTC (Fig. 8e). This rain ($> 18\,\mathrm{mm\,h^{-1}}$) and wind structure are characteristic of deep convection, and are consistent with the cloud structure observed in Fig. 6c.

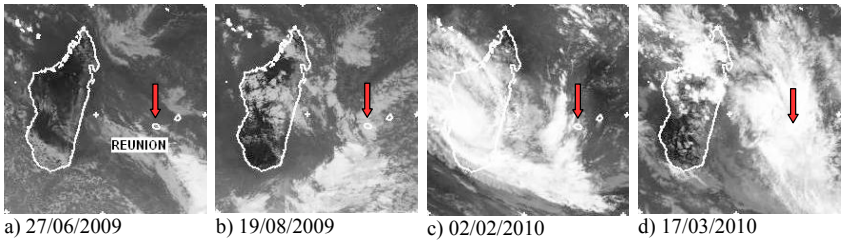

Fig. 6. Thermal infrared (10.5–12.5 µm) Meteosat VISSR (visible and infrared spin-scan radiometer) Indian Ocean data coverage (IODC) images at 12:00 UTC and **(a)** 27 June 2009, **(b)** 19 August 2009 **(c)** 2 February 2010 and **(d)** 17 March 2010.

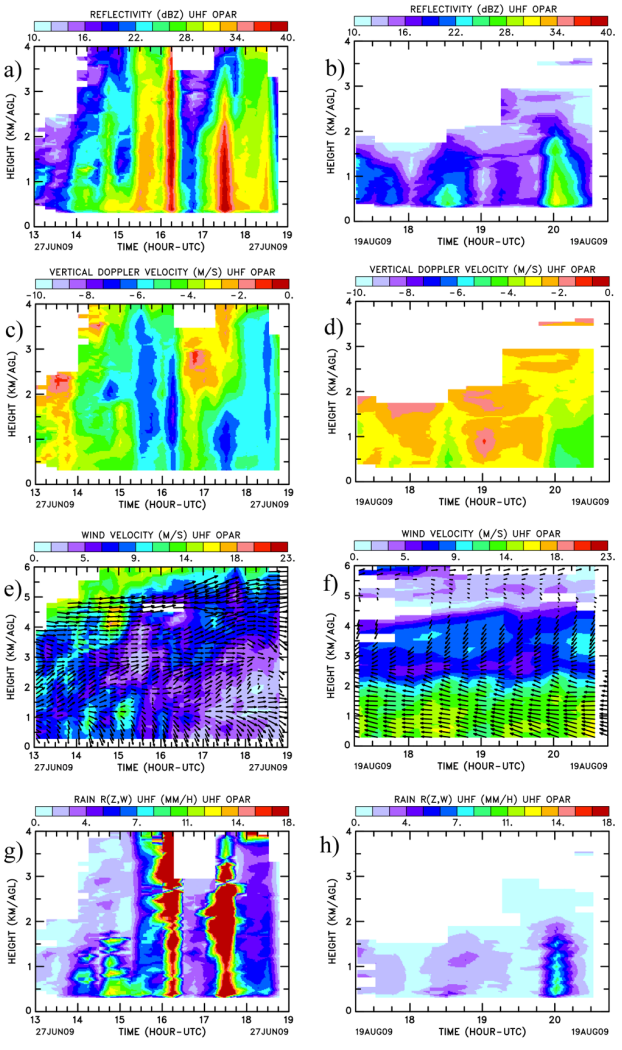

Fig. 7. Time–height sections of reflectivity factor Z **(a, b)**, vertical velocity W **(c, d)**, horizontal wind V intensity and direction **(e, f)** and precipitation rate R **(g, h)** on 27 June 2009 (left panel) and 19 August 2009 (right panel). A 15 min average is used. Note that in **(e–f)** there are more data, since all the data was taken into account.

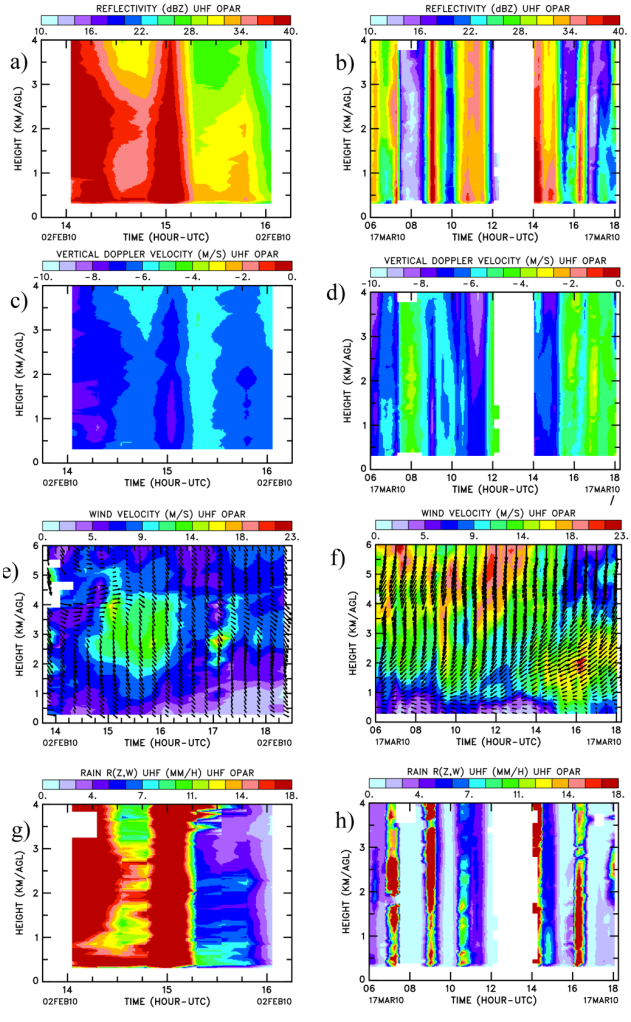

Fig. 8. As in Fig. 7 but for 2 February 2010 (left panel) and 17 March 2010 (right panel).

The NNE case on the 17th march is characterized by less intense precipitation, but is associated with short pulses of very intense precipitation. Reflectivity, vertical Doppler velocity and horizontal wind measurements show significant variability, with values ranging from 10 to 40 dBZ, from −3 to −9 m s^{-1} and from 2 to 23 m s^{-1}, respectively. The vertical structure of the wind (Fig. 8f) indicates the presence of strong horizontal winds at all altitudes. A directional wind shear could be noticed with easterlies below 1 km progressively veering to northerly at 4 km a.m.s.l. In that case, the rain rate attains 18 mm h^{-1} in short durations (∼ 15 min) and shows more variability with height.

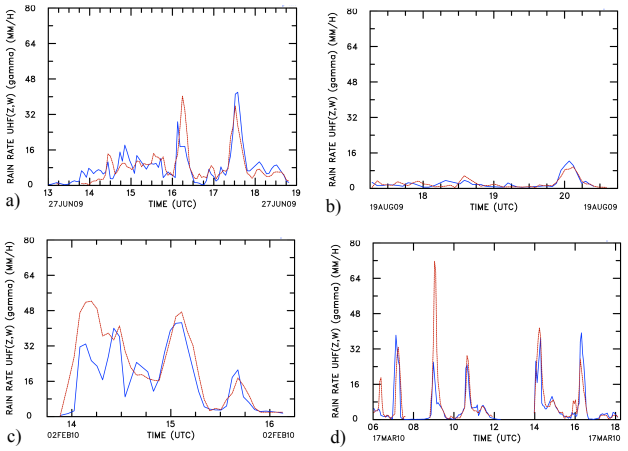

Fig. 9. Time series of rain rate (mm h^{-1}) deduced from UHF profiler data (blue line) between 400 m and 500 m and for **(a)** 27 June 2009, **(b)** 19 August 2009, **(c)** 2 February 2010 and **(d)** 17 March 2010. Red lines show corresponding rain-gauge estimates at sea-level.

The radar-derived rain rates obtained between 400 m and 500 m for each of these events are compared against surface rain gauge measurements over the same observation period (Fig. 9). Overall, both data sets are in excellent agreement whatever the considered weather pattern is, indicating that accurate quantitative information can be inferred from the analysis of wind profiler data. This potentially allows for the investigation of the effect of precipitation on soil erosion through estimating and analysing kinetic energy fluxes deduced from profiler-derived DSD and wind data.

The vertical and horizontal kinetic energy fluxes are estimated from Eqs. (8) and (9). The time–height contours of these fluxes are presented in Fig. 10 for each of the four weather events. Clearly, the horizontal kinetic energy fluxes exceed vertical kinetic energy fluxes by a factor of 5–10 for all four rain systems. This suggests that the erosion process depends more on HKEF than on VKEF. A good agreement between the reflectivity pattern and VKEF can also be seen for all weather situations. Large values of VKEF are associated with strong reflectivities, meaning that weather patterns yielding to convective rain (LP, frontal and NNE) produce larger VKEF. The HKEF is found to be an order of magnitude larger than VKEF on 19 August 2009. The magnitude of both VKEF and HKEF is relatively small compared to that observed in other cases.

The relationship between the VKEF and radar reflectivity factor has been computed for all four cases from a soil-erosion point of view. A linear regression analysis was performed to derive a relationship between these parameters under the form VKEF $= \alpha Z^{\beta}$ (where α and β are searched coefficients). As expected from the previous discussion, the correlation coefficient is extremely high and always exceeds 0.99 (Fig. 11). The retrieved value of α varies slightly between the cases, from 0.0257 to 0.0398 and $\beta = 0.9$. Steiner

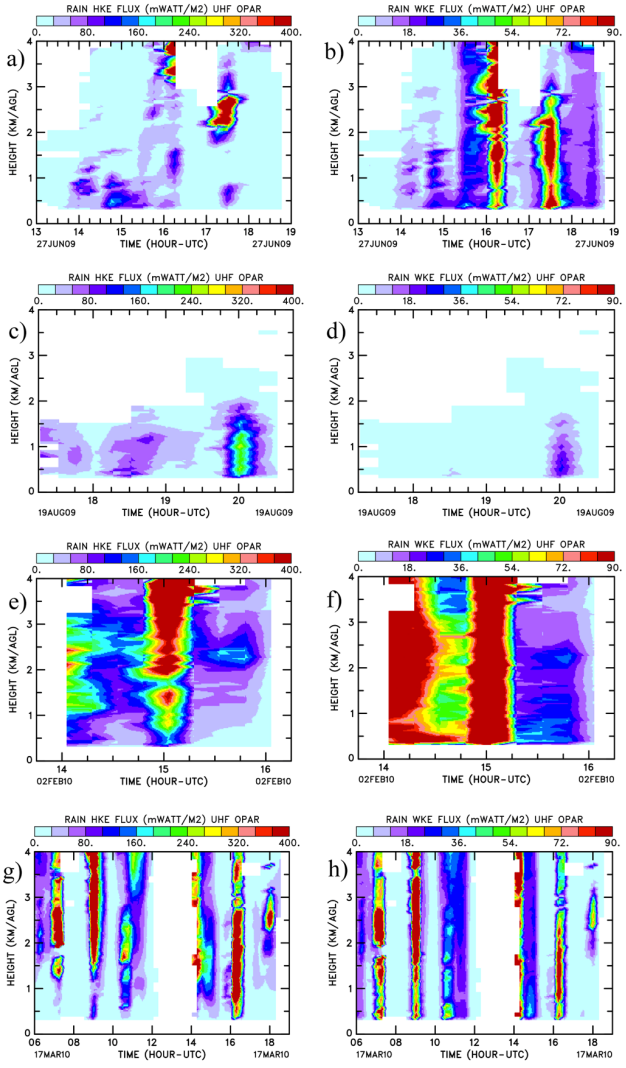

Fig. 10. Time–height sections of the rain horizontal (HKEF, left panel) and vertical (VKEF, right panel) kinetic energy flux for **(a, b)** 27 June 2009, **(c, d)** 19 August 2009, **(e, f)** 2 February 2010 and **(g, h)** 17 March 2010. A 15 min average is used.

and Smith (2000) found a similar climatological relationship for northern Mississippi, based on 1 min raindrop spectra observations; in their study, $Z = 25E^{1.1}$ (i.e., $E = 0.055Z^{0.9}$), which is quite close to the values obtained in the present study.

5 Summary and perspectives

The climatological properties of rainfall during the moist and dry seasons in Réunion were investigated using one year (May 2009–April 2010) of UHF wind profiler and rain gauge observations collected at Saint-Denis international airport. During the dry season (May to October) precipitation is weak (< 2.5 mm h^{-1}) and is generally restricted to the first three kilometres of the atmosphere. The vertical extension of the

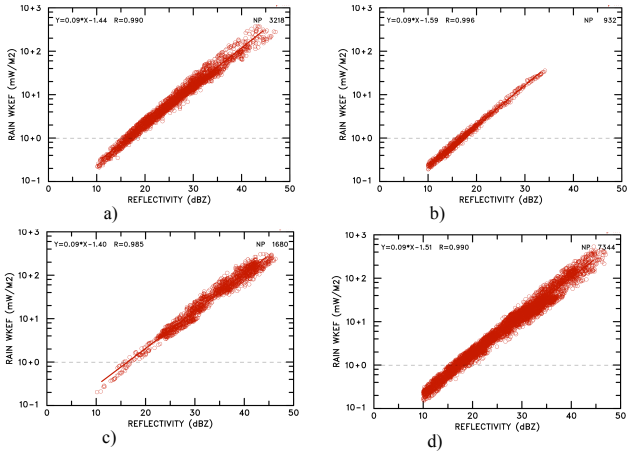

Fig. 11. Vertical kinetic energy flux VKEF, as a function of instantaneous reflectivity factor for **(a)** 27 June 2009, **(b)** 19 August 2009, **(c)** 2 February 2010 and **(d)** 17 March 2010.

clouds is limited either by the inversion of the boundary layer or by the trade wind inversion. In strong trade wind situations, the clouds do not overpass the height of trade wind inversion located around 3000 m. In weak trade wind situations, the clouds are more convectively driven and their vertical extension is determined by the entrainment layer of the boundary layer located around 2 km. Such differences result in larger rain/rain rate variability above 2 km. During the wet season (November to April), the island is affected by northerly to northeasterly flow associated with more or less intense convection, as well as by tropical depression associated with strong precipitation and wind shear. These weather patterns generate more intense ($\sim 5\,\mathrm{mm\,h^{-1}}$) precipitation extending higher than during the dry season.

The dynamical and microphysical characteristics, including drop size distributions, of four rainfall events representative of the variety of precipitating systems occurring in Réunion during both warm and dry seasons were also investigated. For all weather events, the radar-derived rain parameters were in good agreement with those inferred from the analysis of collocated rain gauge observations. Results obtained in these cases studies corroborate those of the climatological analysis, both in terms of precipitation intensity and vertical development.

Vertical and horizontal kinetic energy fluxes were estimated from DSD and wind data to help quantify the effect of precipitation on soil erosion. Computed horizontal kinetic fluxes appear systematically higher than vertical kinetic energy fluxes, which suggests that the erosion process depends more on HKEF than on VKEF. The vertical kinetic energy fluxes are moreover strongly related to the reflectivity. It is concluded that the use of power-law relationships is a viable option for simplifying VKEF (rainfall) estimation procedures.

The analysis of observations collected at Saint-Denis, Réunion demonstrates that accurate qualitative and quantitative information on the structure and intensity of precipitation can be inferred from the analysis of wind profiler data, allowing for the investigation of the effect of precipitation on soil erosion. The next steps will be to achieve a statistical analysis of the horizontal and vertical kinetic energy fluxes for the dry and wet seasons (to construct more robust relationships between these fluxes and the reflectivity factor), as well as to investigate potential relationships between the drop falling angle, the slope of the terrain and rain erosivity. The information on the vertical structure of precipitation and DSD deduced from wind profiler observations is also potentially useful to improve weather radar rainfall estimates and will be further investigated to improve radar quantitative precipitation estimates over the island of Réunion.

Acknowledgements. We acknowledge Meteo France for providing the mean precipitation in Réunion as well as rain rate time series. Particularly, we want to thank the climatology team (Guillaume Jumeaux and François Bonnardot) for their great help in providing the distinct classes of weather patterns representative of the variety of rainfall events in Réunion. We want also to acknowledge Cheikh Dione, Christelle Barthe, Jean Marc Metzger and Soline Bielli for their great help. We acknowledge also Hélène Ferré, Yann Courcoux, Serge Prieur and Franck Gabarrot for radar data collection and management. To finish, we would like to thank the reviewers for their constructive suggestions to improve the quality of the manuscript.

Edited by: F. S. Marzano

The publication of this article is financed by CNRS-INSU.

References

Atlas, D., Srivastava, R. C., and Sekkon, R. S.: Doppler radar characteristics of precipitation at vertical incidence, Rev. Geophys. Space, 2, 1–35, 1973.

Augstein, E., Riehl, H., Ostapoff, F., and Wagner, V.: Mass and energy transports in an undisturbed Atlantic trade-wind flow, Mon. Weather Rev., 101, 101–111, 1973.

Baldy, S., Ancellet, G., Bessafi, M., Badr, A., and Lan Sun Luk, D.: Field observations of the vertical distribution of tropospheric ozone at the island of Réunion (southern tropics), J. Geophys. Res., 101, 23835–23849, doi:10.1029/95JD02929, 1996.

Barcelo, A., Robert, R., and Coudray, J.: A major rainfall event: The 27 February–5 March 1993 rains on the southeastern slope of Piton de la Fournaise Massif (Reunion island, Southwest Indian Ocean), Mon. Weather Rev., 125, 3341–3346, 1997.

Brian, R. B.: Soil erodibility and processes of water erosion on hillslope, Geomorphology, 32, 385–415, 2000.

Chu, Y.-H. and Su, C.-L.: An investigation of the slope-shape relation for gamma raindrop size distribution, J. Appl. Meteorol. Climatol., 47, 2531–2544, 2008.

Cifelli, R., Williams, C. R., Rajopadhyaya, D. K., Avery, S. K., Gage, K. S., and May, P. T.: Drop-size distribution characteristics in tropical mesoscale convective systems, J. Appl. Meteorol., 39, 760–777, 2000.

Clark, W. L., Williams, C. R., Johnston, P. E., Gage, K. S., and Tokay, A.: Reflectivity dependence of reflectivity gradients observed by radar profilers, Preprints, 32nd Conf. on Radar Meteorology, Albuquerque, NM, Am. Meteorol. Soc., P6R.6, available at: http://ams.confex.com/ams/pdfpapers/96646.pdf (last access: 3 February 2014), 2005.

Foote, N. H. and du Toit, P. S.: Terminal velocity of raindrop aloft, J. Appl. Meteorol., 8, 585–591, 1969.

Gossard, E.: Measuring drop-size distributions in clouds with a clear-air-sensing Doppler radar, J. Atmos. Ocean Tech., 5, 640–649, 1988.

Gossard, E., Strauch, R. G., and Rogers, R. R.: Evolution of drop-size distribution in liquid precipitation observed by ground-based Doppler radar, J. Atmos. Ocean. Technol., 7, 815–828, 1990.

Hastenrath, S.: Climate Dynamics of the Tropics, Springer, 244 pp., ISBN 978-0-7923-1346-5, 1991.

Iserloh, T., Fister, W., Marzen, M., Seeger, M., Kuhn, N. J., and Ries, J. B.: The role of wind-driven rain for soil erosion – An experimental approach, Z. Geomorphol., 57, 193–201, 2013.

Johnson, R. H. and Bresch, J. F.: Diagnosed characteristics of precipitation systems over Taiwan during the May–June 1987 TAMEX, Mon. Weather Rev., 119, 2540–2557, 1991.

Kanofsky, L. and Chilson, P. B.: An analysis of errors in drop size distribution retrievals and rain bulk parameters with a UHF wind profiling radar and a two-dimensional video disdrometer, J. Atmos. Ocean. Tech., 25, 2282–2292, 2008.

Kinnell, P. I. A.: Raindrop-impact-induced erosion processes and prediction: A review, Hydrol. Process., 19, 2815–2844, 2005.

Kozu, T. and Nakamura, K.: Rainfall Parameter Estimation from Dual-Radar Measurements Combining Reflectivity Profile and Path-Integrated Attenuation, J. Atmos. Ocean. Tech., 8, 259–270, 1991.

Lesouëf, D.: Ph. D thesis: Numerical studies of local atmospheric circulations over Reunion island: application to the dispersion of pollutants, available at: http://tel.archives-ouvertes.fr/tel-00633096 (last access: 3 February 2014), 2010.

Lesouëf, D., Gheusi, F., Delmas, R., and Escobar, J.: Numerical simulations of local circulations and pollution transport over Reunion Island, Ann. Geophys., 29, 53–69, doi:10.5194/angeo-29-53-2011, 2011.

Postel, G. A. and Hitchman, M. H.: A Case Study of Rossby Wave Breaking along the Subtropical Tropopause, Mon. Weather Rev., 129, 2555–2569, 2001.

Quetelard, H., Bessemoulin, P., Cerveny, R. S., Peterson, T.,C., Burton, A., and Boodhoo, Y.: World record rainfalls (72-hour and four-day accumulations) at Cratère Commerson, Réunion island, during the passage of Tropical Cyclone Gamede, B. Am. Meteorol. Soc., 90, 603–608, 2009.

Rajopadhyaya, D. K., May, P. T., and Vincent, R. A.: A general approach to the retrieval of rain drop size distributions from wind profiler Doppler spectra: Modelling results, J. Atmos. Ocean. Tech., 10, 710–717, 1993.

Rao, T. N., Kirankumar, N. V. P., Radhakrishna, B., Rao, D. N., and Nakamura, K.: Classification of tropical precipitating systems using wind profiler spectral moments. Part I: Algorithm description and validation, J. Atmos. Ocean. Tech., 25, 884–897, 2008.

Rao, T. N., Radhakrishna, B., Nakamura, K., and Prabhakara Rao, N.: Differences in raindrop size distribution from southwest monsoon to northeast monsoon at Gadanki, Q. J. Roy. Meteorol. Soc., 135, 1630–1637, 2009.

Riehl, H.: Tropical Meteorology, McGraw-Hill, 392 pp., 1954.

Romkens, M. J. M., Prasad, S. N., and Whisler, F. D.: Surface sealing and infiltration, in: Process Studies in Hillslope Hydrology, edited by: Anderson, M. G. and Burt, T. P., Wiley, Chichester, 1990.

Rosenfeld, D. and Ulbrich, C. W.: Cloud microphysical properties, processes, and rainfall estimation opportunities, Meteorol. Monogr., 30, 237–258, 2003.

Sanderson, M. (Ed.): Prevailing Trade-winds, Weather and Climate in Hawaii, University of Hawaii Press, 126 pp., 1993.

Schafer, R., Avery, S., May, P., Rajopadhyaya, D., and Williams, C.: Estimation of rainfall drop size distributions from dual- frequency wind profiler spectra using deconvolution and a nonlinear least squares fitting technique, J. Atmos. Ocean. Tech., 19, 864–874, 2002.

Smith, R. B., Minder, J. R., Nugent, A. D., Storelvmo, T., Kirshbaum, D. J., Warren, R., Lareau, N., Palany, P., James, A., and French, J.: Orographic Precipitation in the Tropics: The Dominica Experiment, B. Am. Meteorol. Soc., 93, 1567–1579, doi:10.1175/BAMS-D-11-00194.1, 2012

Steiner, M. and Smith, J. A.: Reflectivity, rain rate, and kinetic energy flux relationships based on raindrop spectra, J. Appl. Meteorol., 39, 1923–1940, 2000.

Stevens, B.: On the growth of layers of nonprecipitating cumulus convection, J. Atmos. Sci., 64, 2916–2931, 2007.

Su, C. L. and Chu, Y. H.: Analysis of Terminal Velocity and VHF Backscatter of Precipitation Particles Using Chung-Li VHF Radar Combined with Ground-Based Disdrometer, Terr. Atmos. Ocean. Sci., 18, 97–116, 2007.

Taupin, F. G., Bessafi, M., Baldy, S., and Bremaud, P. J.: Tropospheric ozone above the southwestern Indian Ocean is strongly linked to dynamical conditions prevailing in the tropics, J. Geophys. Res., 104, 8057–8066, doi:10.1029/98JD02456, 1999.

Ulbrich, C. W.: Natural variations in the analytical form of the raindrop size distribution, J. Clim. Appl. Meteorol., 22, 1764–1775, 1983.

Ulbrich, C. W. and Atlas, D.: Rainfall microphysics and radar properties: Analysis methods for drop size spectra, J. Appl. Meteorol., 37, 912–923, 1998.

Wakasugi, K., Mizutani, A., Matsuo, M., Fukao, S., and Kato, S.: A direct method for deriving drop-size distributiona and vertical air velocities from VHF Doppler radar spectra, J. Atmos. Ocean. Tech., 3, 623–629, 1986.

Williams, C. R.: Simultaneous ambient air motion and raindrop size distributions retrieved from uhf vertical incident profiler observations, Radio Sci., 37, 8.1–8.16, doi:10.1029/2000RS002603, 2002.